Dalton Transactions

ROYAL SOCIETY OF CHEMISTRY

PAPER

View Article Online
View Journal | View Issue

Cite this: *Dalton Trans.*, 2025, **54**, 11925

Zinc(II), copper(II) and silver(I) salicylate-metronidazole complexes as novel antimicrobial agents†

Laura Contini, [a] Raymond J. Turner *[b] and Fabrizia Grepioni *[a]

Received 8th May 2025,
Accepted 10th July 2025

DOI: 10.1039/d5dt01086a

rsc.li/dalton

Combining zinc(II), copper(II) and silver(I) salicylates with metronidazole through *via* mechanochemistry and slurry, leads to the formation of the new metal complexes $[Zn(Sal)_2(MET)_2]$ Form I (**1a**), $[Zn(Sal)_2(MET)_2]$ Form II (**1b**), $[Cu(Sal)_2(MET)_2(H_2O)]$ Form I (**2a**), $[C(Sal)_2(MET)_2\ (H_2O)]$ Form II (**2b**) and[Ag(Sal)(MET)] (**3**), that have been fully characterized *via* single crystal and powder X-ray diffraction and thermal techniques. Antimicrobial assays conducted on the thermodynamically stable forms of polymorphic zinc(II) and copper(II) complexes and the silver complex, have demonstrated that these complexes behave as effective agents against both Gram-positive and Gram-negative bacteria, including biofilm-forming strains, and evidence the potential application of crystal engineering strategies to modify and improve existing drugs in confronting the growing threat of antimicrobial resistance; our results are particularly promising if one considers the limited antimicrobial activity of pure metronidazole against aerobic pathogens.

Introduction

Antimicrobial resistance (AMR) is a phenomenon that arises when microbes – viruses, bacteria and fungi – evolve under selective pressure and no longer respond to antimicrobial treatments that were once effective.[1,2] Microbes evolve, over time and exposure, to develop resistance to any stressors, but this natural evolutionary process has been drastically accelerated by the misuse and overuse of antimicrobial agents in humans, animals and agriculture.[3–5] As a result, AMR now represents one of the most pressing global threats to public health and sustainable development.[6] In 2019 alone, bacterial AMR was directly responsible for an estimated 1.27 million deaths worldwide.[7] The economic burden is similarly alarming: the World Bank estimates that AMR could lead to an additional US$ 1 trillion in healthcare costs by 2050 and annual gross domestic product (GDP) losses ranging from US$ 1 trillion to US$ 3.4 trillion by 2030.[8]

The most effective strategies to combat AMR include reducing antibiotic misuse and investing in the development of new therapeutic agents. However, it cannot be overlooked that the current clinical pipeline remains insufficient to meet this challenge.[9] According to a 2024 World Health Organization (WHO) analysis, as of December 2023 only 57 antibiotics and 40 non-traditional antibacterials were in clinical development (Phases I–III), and just 38% of these candidates were considered truly innovative.[10] Given the urgency, novel approaches to developing antibacterials are thus needed.

One such approach lies in the exploration of metal-based antimicrobials.[11,12] Inorganic and organometallic compounds have played a limited, yet crucial role in 20th-century medicine. The discovery and approval of the anticancer drug cisplatin marked the beginning of medicinal inorganic chemistry.[13] Since then, numerous metal-containing compounds have been explored for treating various diseases, with some of them progressing to clinical (human) trials.[14–18] However, it is only recently, in response to the alarming rise of AMR over the past decade, that metals and metalloantimicrobials[19] or metalloantibiotics[20] have garnered a resurgent interest as potential new antimicrobials.[11,21–23] Such interest stems from the structural and chemical tunability provided by coordination chemistry, which enables the possibility of expanding the chemical space of antibiotic development beyond the constraints of classical drug design.[23] Indeed, a rational choice of the components of the metal complex could enable the modulation of the metal–ligand interactions, enhancing the antimicrobial efficacy while mitigating cytotoxicity.[24]

A key advantage of metalloantibiotics lies in their multimodal mechanisms of action, including the generation of reactive oxygen species (ROS), interference with metalloprotein function, and the introduction of membrane stress.[25–27] These

[a]*Dipartimento di Chimica "Giacomo Ciamician", Università di Bologna, via Gobetti 85, 40129 Bologna, Italy. E-mail: fabrizia.grepioni@unibo.it*
[b]*Department of Biological Sciences, University of Calgary, Canada. E-mail: turnerr@ucalgary.ca*

†Electronic supplementary information (ESI) available: Powder X-ray diffraction patterns, crystal data, DSC and TGA traces, antimicrobial activity tests, Hirshfeld surface analysis. CCDC 2448808–2448812. For ESI and crystallographic data in CIF or other electronic format see DOI: https://doi.org/10.1039/d5dt01086a

multimodal mechanisms introduce a higher evolutionary barrier to resistance development, as bacterial adaptation to one mechanism does not confer protection against others.

Among existing antimicrobial, metronidazole (MET), a nitroimidazole derivative introduced in the 1960s, remains a frontline treatment for anaerobic protozoan and bacterial infections.[28] While initially employed against *Trichomonas vaginalis*, it has since proven effective against *Helicobacter pylori*, *Clostridium difficile*, *Entamoeba histolytica*, and *Giardia lamblia*, *among others*. However, emerging resistance to MET has been identified in multiple pathogens, raising concerns about its continued effectiveness and prompting efforts to repurpose it for modern therapeutic challenges.[29,30] In this work, we applied crystal engineering strategies to develop metal–metronidazole complexes with enhanced antimicrobial activity with the final aim of repurposing the antibiotic against resistant strains of microbes.[31–36] The preparation of co-crystals of known drugs,[37–39] as well as the co-crystallization of natural antibacterials with metal salts,[40–43] have been shown to be successful in a number of cases.[44]

In the case of metronidazole, however, recent work by Braun *et al.*[36] evidences the difficulties of obtaining organic cocrystals of this active principle. We therefore decided to investigate the antimicrobial properties of MET (see Chart 1) resulting from coordination complexes formation, combining it with zinc, copper, and silver salicylates. Zinc and copper are widely known and used for their antimicrobial properties in diverse fields,[45–48] although the lion's share, especially in the antibacterial field, is taken by silver,[49–52] despite indications of rising resistance in some bacterial strains.[53–55]

The use of salicylate as a co-ligand might enhance the efficacy of the antibacterial response.[56] By leveraging both the known pharmacological profile of metronidazole and the unique antimicrobial properties of metal ions, we aim to develop new antimicrobials.

The following complexes were synthesised *via* solution or solid-state methods (see Experimental): $[Zn(Sal)_2(MET)_2]$ Form I (**1a**) and Form II (**1b**), $[Cu(Sal)_2(MET)_2(H_2O)]$ Form I (**2a**) and Form II (**2b**), and [Ag(Sal)(MET)] (**3**). The antimicrobial properties of **1b**, **2b** and **3** were tested against two Gram-positive (*Staphylococcus aureus* ATCC 25923 and *Streptococcus epidermidis* ATCC 12228) and two Gram-negative (*Escherichia coli* ATCC 25922 and *Pseudomonas aeruginosa* ATCC 27853) pathogens.

Chart 1 The reagents used in this work in combination with zinc(II), copper(II) and silver(I).

Experimental

Materials and methods

Metronidazole was purchased from Tokyo Chemical Industries (TCI), the other reagents (see Chart 1) from Sigma–Aldrich; all were used without further purification.

Synthesis

All compounds were synthesized as summarized in Table 1.

Mechanochemical synthesis. The metal complexes **1b**, **2b** and **3** were obtained by mechanochemical reaction of MET (1 mmol) with the salicylate complexes $[Zn(Sal)_2(H_2O)_2]$ (0.5 mmol), $[Cu(Sal)_2(H_2O)_2]$ (0.5 mmol) and [Ag(Sal)] (1 mmol), respectively. Liquid assisted grinding (LAG)[57] was conducted for 90 min in 5 mL stainless steel jars in the presence of 100 μL of H_2O and two 7 mm stainless steel balls, with a Retsch MM400 ball miller operated at the frequency of 25 Hz.

Compounds **1b** and **3** could also be obtained, in the same ball milling conditions, if HSal (1 mmol) and ZnO (0.5 mmol) or $AgNO_3$ (1 mmol) were used instead of the salicylate complexes, as confirmed by powder X-ray diffraction (PXRD) measurements on the solid products, previously washed with H_2O/EtOH at room temperature. When the same reaction was repeated with $CuCl_2{\cdot}2H_2O$ (0.5 mmol), however, an amorphous powder was obtained that, after recrystallization from water at room temperature, yielded a crystalline mixture of **2a** and **2b**, as confirmed by a comparison of the experimental powder pattern with those calculated for **2a** and **2b** on the basis of their single crystal structure (see below).

Slurry synthesis. The metal complexes **1b**, **2b** and **3** were obtained by slurrying stoichiometric amounts of MET (1 mmol), HSal (1 mmol) and either ZnO (0.5 mmol), $CuCl_2{\cdot}2H_2O$ (0.5 mmol) or $AgNO_3$ (1 mmol) in 500 μL of water. The same products were obtained by substituting HSal and the metal salt with the corresponding salicylate complex, namely $[Zn(Sal)_2(H_2O)_2]$, $[Cu(Sal)_2(H_2O)_2]$ and [Ag(Sal)], respectively. In both cases the products obtained were washed with water and ethanol, to remove unreacted reagents, and characterized *via* powder X-ray diffraction (PXRD).

Table 1 Summary of the synthetic methods employed for the synthesis of the complexes studied in this work

Compound	Synthetic method
$[Zn(Sal)_2(MET)_2]$ Form I (**1a**)	Solution reaction
$[Zn(Sal)_2(MET)_2]$ Form II (**1b**)	Slurry/LAG[a], SCSC[b] conversion from **1a**, grinding of **1a**
$[Cu(Sal)_2(MET)_2(H_2O)]$ Form I (**2a**)	LAG[c]
$[Cu(Sal)_2(MET)_2(H_2O)]$ Form II (**2b**)	Slurry/LAG[a]
[Ag(Sal)(MET)] (**3**)	Slurry/LAG[a]

[a] Recrystallization of powder products yielded crystals suitable for single crystal X-ray diffraction. [b] Single-crystal-to-single-crystal (SCSC) transformation. [c] Recrystallization from water yielded a physical mixture of **2a** and **2b**.

Solution synthesis

*The [Zn(Sal)$_2$(MET)$_2$] Form I (**1a**).* MET (1 mmol), HSal (1 mmol) and $Zn(NO_3)_2{\cdot}6H_2O$ (0.5 mmol) were dissolved in water, under reflux, and the solution was kept under reflux for 1 h. The resulting light-yellow, clear solution was cooled to room temperature; single crystals were obtained after few days and analysed *via* single crystal X-ray diffraction (SCXRD). Spontaneous *single-crystal-to-single-crystal* conversion of **1a** over 2 weeks yielded single crystals of **1b**, that were analysed *via* SCXRD.

*[Cu(Sal)$_2$(MET)$_2$(H$_2$O)] Form I (**2a**).* NaSal (1 mmol) and $CuSO_4$ (0.5 mmol) were dissolved in 5 mL of water; a second solution, prepared by dissolving 1 mmol of MET in the minimum amount of water, was then slowly added under stirring. After one week the clear green solution yielded single crystals of **2a**, that were analysed *via* SCXRD.

Recrystallization of powder products. Single crystals of **1b**, **2b** and **3** were obtained by slow evaporation at ambient conditions of an acetone solution of the corresponding LAG products and analysed *via* SCXRD.

Single crystal X-ray diffraction (SCXRD)

Single crystal data for **1a**, **1b**, **2a**, **2b** and **3** were collected at room temperature on an Oxford X'Calibur S CCD diffractometer equipped with a graphite monochromator (Mo-Kα radiation, λ = 0.71073 Å). Reflection data were integrated and elaborated with the CrysAlisPro Software. The structures were solved with SHELXT[58] by intrinsic phasing and refined on F^2 with SHELXL,[59] implemented in the Olex2 software,[60] by full-matrix least squares refinement. H_{OH} atoms were either directly located or, when not possible, added in calculated positions; H_{CH} atoms for all compounds were added in calculated positions and refined riding on their respective carbon atoms. All non-hydrogen atoms were refined anisotropically. One 2-hydroxyethyl group of one of the two MET ligands in **1a** shows a 80 : 20 disorder. One salicylate ligand in **2b** shows a 50 : 50 disorder of the –OH group on opposite sides of the aromatic ring. The same disorder (modelled as 25 : 75) is observed on another salicylate ligand of the same compound (**2b**). Data collection and refinement details are listed in Table ESI-1.† The program Mercury[61] was used for graphic representations. Hirshfeld surfaces[62–64] have also been added to the ESI.†

Crystal data tables are collected in the ESI† file. Crystal data have been deposited with the Cambridge Crystallographic Data Centre, 12 Union Road, Cambridge CB21EZ, UK as supplementary publication No. CCDC 2448808–2448812.

Powder X-ray diffraction (PXRD)

The X-ray diffraction patterns were collected in Bragg–Brentano geometry on a PANalytical X'Pert Pro automated diffractometer, equipped with an X'celerator detector, using Cu-Kα radiation (λ = 1.5418 Å) without monochromator in the 3–40° 2θ range (step size 0.033°; time/step: 20 s; Soller slit 0.04 rad, anti-scatter slit: 1/2, divergence slit: 1/4; 40 mA·40 kV). Phase identification was performed by comparing the experimental powder diffraction patterns with those calculated[61] on the basis of single crystal data.

Thermogravimetric analysis (TGA)

TGA measurements were performed with a PerkinElmer TGA8000 in the 25–700 °C temperature range, under N_2 gas flow at a heating rate of 10 °C min^{-1}. TGA traces are reported in the ESI.†

Differential scanning calorimetry (DSC)

Differential scanning calorimetry (DSC) traces were recorded using a PerkinElmer DSC 8500 apparatus. In a typical procedure, the sample (5–10 mg) was weighed into a DSC aluminium pan and then capped with a lid. All samples were first cooled down to 0 °C, then they were heated, at 10 °C min^{-1}, until the onset of degradation was observed. All the experiments were performed under an N_2 flow with a flow rate of 20 mL min^{-1}. DSC traces are reported in the ESI.†

Antimicrobial activity

The antimicrobial efficacy of [Zn(Sal)$_2$(MET)$_2$] Form II (**1b**), [Cu(Sal)$_2$(MET)$_2$(H$_2$O)] Form II (**2b**) and [Ag(Sal)] (**3**), *i.e.* the thermodynamically stable forms of the synthesized metronidazole-based metal complexes, was determined and compared with that of the starting reagents MET, NaSal, [Zn(Sal)$_2$(H$_2$O)$_2$], [Cu(Sal)$_2$(H$_2$O)$_2$] and [Ag(Sal)]. Antimicrobial efficacy was examined using the standard broth dilution method against the Gram-positive (*Staphylococcus aureus* ATCC 25923 and *Streptococcus epidermidis* ATCC 12228) and Gram-negative (*Escherichia coli* ATCC 25922 and *Pseudomonas aeruginosa* ATCC 27853) as examples of key pathogens. The assay was performed in duplicate using 96-wells plates. The type culture collection indicator strains were used to avoid the variability of laboratory domesticated variants; for this reason they were not subcultured more than twice from the original strain.

The assays were performed using Luria–Bertani broth (LB) as liquid media for microbial growth. LB was prepared from milliQ water with 10 g L^{-1} NaCl, 5 g L^{-1} yeast extract, and 10 g L^{-1} tryptone. The agar medium was prepared by adding 10 g L^{-1} bacteriological agar to the LB prior to autoclaving. Bacterial cultures were initiated from frozen stocks and grown overnight in LB broth at 37 °C with shaking (180 rpm). The bacterial culture was adjusted to 6×10^8 CFU mL^{-1} by comparing to a 2 McFarland standard. Subsequently, 25 µL of the bacterial suspension were diluted in 30 mL of LB broth to achieve a working concentration of 5×10^5 CFU mL^{-1}. Serial two-fold dilutions of the test compounds were prepared in a 96-well plate using LB broth, with a final well volume of 200 µL comprising 100 µL of antimicrobial solution and 100 µL of bacterial inoculum. Positive (bacteria without compound) and negative (broth only) controls were included.

The plates were incubated at 37 °C for 18–20 hours. The MIC (Minimum Inhibitory Concentration) was defined as the lowest concentration of the compound that inhibited visible bacterial growth, assessed both visually and spectrophotometrically (absorbance at 600 nm). Wells without visible growth

were plated on LB agar to determine the MBC (Minimum Bactericidal Concentration), defined as the lowest concentration yielding no colonies (0 CFU) after 20 hours of incubation at 37 °C.

Biofilm inhibition was evaluated on the 96-well plates used for MIC determination. Following the MIC assay, the culture supernatants were carefully removed, and wells were washed with MilliQ water to remove planktonic cells. A fixation step was carried out by adding 300 µL of 98% EtOH, which was then left to evaporate at RT. The plate wells were then washed three times with milliQ water; afterwards a 0.1% crystal violet (CV solution was added to each well and incubated at room temperature for 30 minutes. The CV solution was then decanted, and the wells were washed three times with MilliQ water before being allowed to air-dry. To solubilize the bound CV, 200 µL of 30% acetic acid was added to each well. The extracted CV was quantified spectrophotometrically at an absorbance of 600 nm. Amount of Biofilm material was calculated as a percentage relative to unchallenged control wells.)

Fractional inhibitory concentration index (FICi)

The antibacterial activity of salicylate metal complexes in combination with the antibiotic was evaluated using the broth micro-dilution checkerboard assay in order to establish if the individual compounds of the complexes are synergistic in their antimicrobial activity.[65] Liquid culture of the pathogens used for this assay (*S. epidermidis* and *P. aeruginosa*) were adjusted to 5×10^5 CFU mL^{-1} and inoculated into 96-well plates containing a two-dimensional concentration grid of metronidazole (diluted vertically) and the salicylate metal complex (diluted horizontally). Antibiotic concentrations ranged from 0.25× to 4× the MIC of each compound. After inoculation, a final volume of 100 µL was obtained (50 µL of compounds solution + 50 µL of inoculant). Positive (bacteria only) and sterility (broth only) controls were included. Plates were incubated at 37 °C for 18–20 hours without shaking. MIC values for antibiotics in combination were determined as the lowest concentration of each compound at which visible growth was inhibited. FIC indices were calculated using the formula:

$$FIC_A = \frac{MIC_A \text{ in combination}}{MIC_A \text{ alone}}$$

$$FIC_B = \frac{MIC_B \text{ in combination}}{MIC_B \text{ alone}}$$

$$FIC_i = FIC_A + FIC_B$$

FIC indices were interpreted as synergistic ($FIC_i \leq 0.5$), additive ($FIC_i > 0.5$ to ≤ 1.0), indifferent ($FIC_i > 1.0$ to ≤ 4.0), or antagonistic ($FIC_i > 4.0$).[66] Assays were performed in biological triplicates and results expressed as mean FIC_i value.

Results and discussion

Preparation and characterization of $[Zn(Sal)_2(MET)_2]$

The two distinct polymorphs of the zinc(II) complex $[Zn(Sal)_2(MET)_2]$, **1a** and **1b**, were obtained through different synthetic methods (Scheme 1). Synthesis from solution consistently yielded the polymorph **1a**. In contrast, bulk synthesis, *i.e.* mechanochemical and slurry, yielded the polymorphic form **1b**, irrespective of the starting material choice (ZnO or a preformed zinc salicylate complex).

Interestingly, **1a** spontaneously transformed into **1b** through a single-crystal-to-single-crystal conversion in a matter of two weeks, indicating that **1b** is the thermodynamically stable polymorph at room temperature. Conversion from **1a** to **1b** also occurs in a matter of minutes upon grinding single crystals of **1a** (see Fig. ESI-1†). Single crystals of **1b** were also obtained from the recrystallization in acetone of the powder product. The structure of both polymorphs was solved *via* SCXRD. Structural characterization of the LAG and slurry products was done by comparing the experimental powder diffraction patterns with the calculated ones for forms **1a** and **1b** (see Fig. ESI-2 and 3†).

SCXRD revealed that both polymorphs feature a tetra-coordinated zinc(II) centre, with two metronidazole (MET) molecules and two salicylate (Sal) anions coordinating the metal ion in a tetrahedral fashion. The orientation of the MET ligands around the N–Zn bonds in **1a** and **1b** is markedly different (see Fig. 1), and the conformations of the MET ligands also differ (see Fig. ESI-7†). This differences significantly influence the hydrogen-bonding network within the crystal structures, and accounts for the different packing arrangements of the two forms (Fig. 2). The smaller unit cell volume of **1b** with respect to **1a** indicates a more efficient

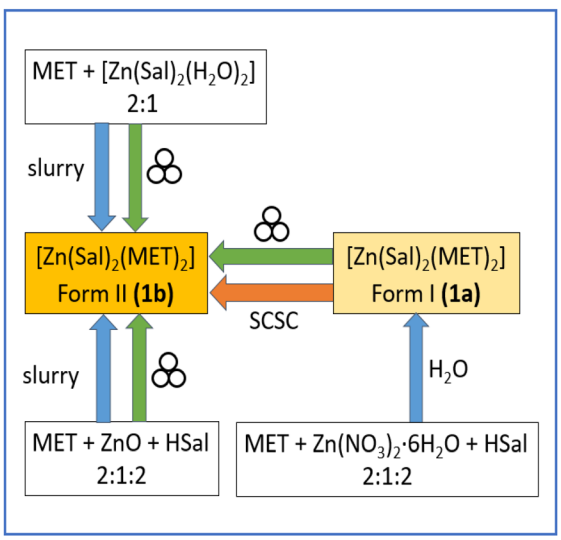

Scheme 1 Details of the LAG, slurry and crystallization processes for the synthesis of $[Zn(Sal)_2(MET)_2]$ (**1**) from various precursors, and details of polymorphic transition between Form I (**1a**) and Form II (**1b**).

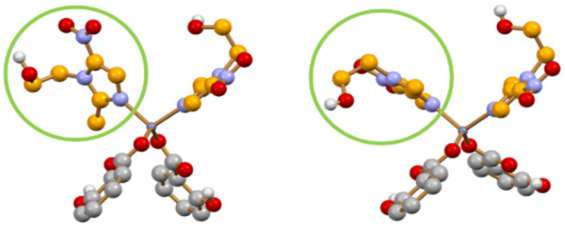

Fig. 1 Different orientation of the MET ligands around the N–Zn bonds in $[Zn(Sal)_2(MET)_2]$ **1a** (left) and **1b** (right) [C_{MET} in orange, C_{Sal} in grey; H_{CH} atoms not shown for clarity.].

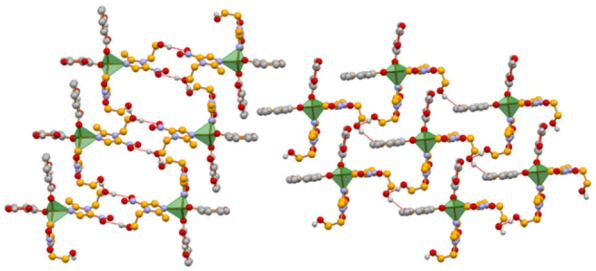

Fig. 2 Comparison of the H-bonding pattern choices resulting from the different MET orientation in crystalline $[Zn(Sal)_2(MET)_2]$ **1a** (left) and **1b** (right) [C_{MET} in orange, C_{Sal} in grey; H_{CH} atoms not shown for clarity.].

packing in the solid state and is in agreement with the higher thermodynamic stability of **1b**. Because of its higher stability and the ease of preparation in bulk form *via* solid-state techniques, further characterizations have been carried out only on **1b**.

Thermal stability of **1b** was assessed *via* TGA and DSC measurements (see Fig. ESI-9 and 10†). TGA was performed in the 30–650 °C range; the metal complex is stable up to 130 °C where a multistep degradation occurs, which ends at 550 °C. DSC was performed in the 20–130 °C range and no thermal event was observed in such range.

Preparation and characterization of $[Cu(Sal)_2(MET)_2(H_2O)]$

Polymorphism was also observed for the copper complex, with Form I (**2a**) and Form II (**2b**) resulting from different synthetic routes and starting copper(II) source (Scheme 2).

Solution methods yielded single crystals of **2a**, while slurry synthesis consistently yielded **2b** in powder form, regardless of whether the starting material was a copper salt or a pre-formed copper salicylate complex (Fig. ESI-4 and 5†). The influence of the starting copper source was observed, however, when the synthesis was performed mechanochemically *via* Liquid Assisted Grinding (LAG): the use of copper bis-salicylate resulted in the obtainment of pure **2b**, whereas the reaction $CuCl_2$ and sodium salicylate (see Materials and methods) resulted in a physical mixture of **2a** and **2b** (Fig. ESI-4†).

Both polymorphs feature a penta-coordinated copper(II), with two metronidazole (MET) molecules, two salicylate (Sal) anions and one water molecule coordinating the metal centre

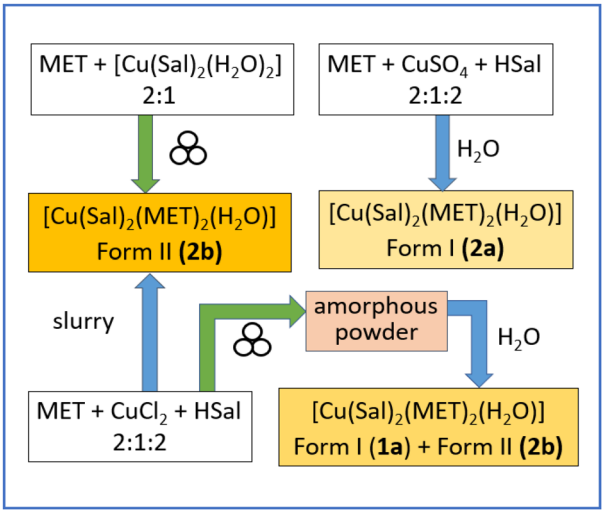

Scheme 2 Details of the LAG, slurry and crystallization processes for the synthesis of $[Cu(Sal)_2(MET)_2(H_2O)]$ (**2**) from various precursors.

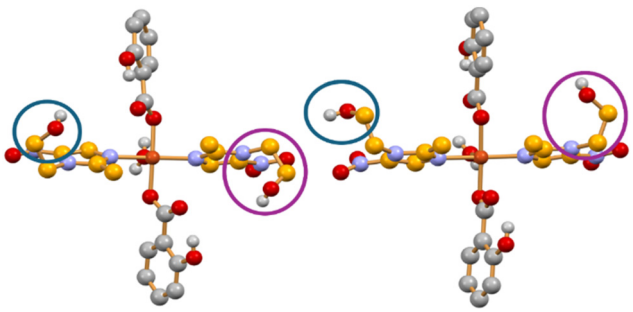

Fig. 3 Different orientation of the MET ligands around the N–Cu bonds in $[Cu(Sal)_2(MET)_2(H_2O)]$ **2a** (left) and **2b** (right) [C_{MET} in orange, C_{Sal} in grey; H_{CH} atoms not shown for clarity.].

(Fig. 3). As observed for the zinc complex, the two polymorphs differ both for the orientation of the two metronidazole molecules around the N–Cu bonds and for the MET molecules conformation (see Fig. ESI-8†). Despite these differences, the packing arrangement is similar in the two crystal forms (Fig. 4).

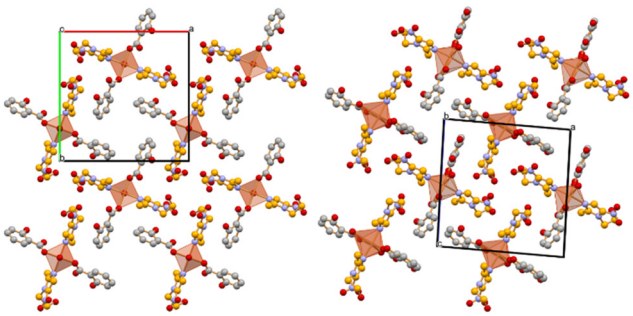

Fig. 4 Packing arrangement of the metal complexes in [Cu $(Sal)_2(MET)_2(H_2O)$] **2a** (left) and **2b** (right) [C_{MET} in orange, C_{Sal} in grey; H atoms not shown for clarity.].

As in the case of the zinc complex, the higher thermodynamic stability of **2b** is reflected in the smaller unit cell volume with respect to **2a**, indicating a more efficient packing in the solid state. Because of its higher stability and the ease of preparation in bulk form with solid-state techniques, further characterizations have been carried out only on [Cu(Sal)$_2$(MET)$_2$(H$_2$O)] **2b**.

Thermal stability of **2b** was assessed *via* TGA and DSC measurements (see Fig. ESI-9 and 10†). TGA was performed in the 30–700 °C range; in agreement with the monohydrate nature of the compound, an initial weight loss occurs at *ca.* 70 °C, which is ascribable to the loss of the coordinated water molecule. The anhydrous metal complex is then stable up to 160 °C, where a multistep degradation occurs. Degradation ends at 600 °C. DSC was performed in the 20–160 °C range. The trace shows an initial broad endothermic peak at 100 °C, corresponding to the first weight loss observed in TGA, and thus attributed to dehydration. A second, smaller endothermic peak (most probably involving the anhydrous complex, which has not been characterized), has been observed prior to degradation at 140 °C.

[Ag(Sal)(MET)]

In contrast to the zinc and copper complexes, the silver compound [Ag(Sal)(MET)] (**3**) did not exhibit polymorphism under the studied conditions. The same product was obtained across all synthetic methods (Scheme 3).

Recrystallization from acetone of the compound in powder form yielded single crystals of the complex, which were then used for the structural characterization *via* SCXRD. The two crystallographically independent silver complexes form large dimeric rings and hydrogen bonded infinite chains, respectively (Fig. 5).

Thermal stability of **3** was assessed *via* TGA and DSC measurements (see Fig. ESI-9 and 10†). TGA was performed in the 30–700 °C thermal range. The metal complex is stable up to 160 °C, then a multistep degradation occurs that ends at 490 °C. DSC was performed in the thermal range of stability of the compound, between 20 °C and 160 °C; no thermal event was observed in the analysed range.

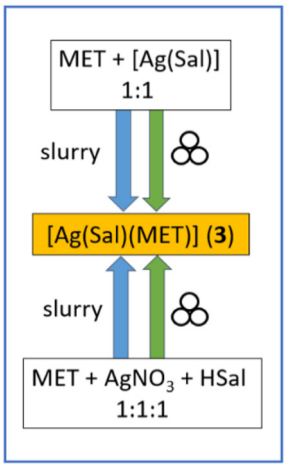

Scheme 3 Details of the LAG and slurry processes for the synthesis of [Ag(Sal)(MET)] (**3**) from various precursors.

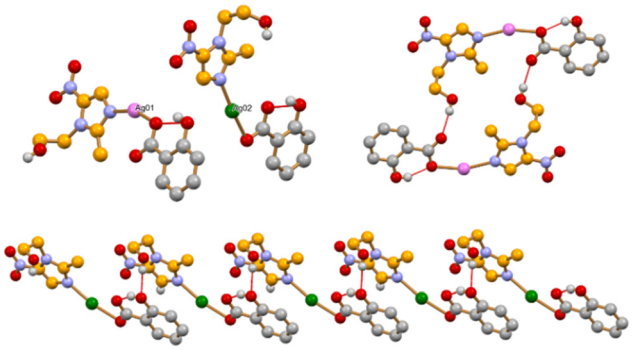

Fig. 5 Linear coordination around the two independent silver(I) cations in [Ag(Sal)(MET)] (**3**) (top left); hydrogen bonds link the two independent units in dimers (top right) and infinite chains extending parallel to the crystallographic *a*-axis (bottom) [Pink and green spheres indicate the two independent silver cations. C_{MET} in orange, C_{Sal} in grey; H_{CH} atoms not shown for clarity.].

Antimicrobial efficacy

The antimicrobial activity of the metal complexes **1b**, **2b** and **3** was assessed against four bacterial strains: the Gram-negative species *Escherichia coli* and *Pseudomonas aeruginosa*, and the Gram-positive *Staphylococcus aureus* and *Staphylococcus epidermidis*. Minimum inhibitory concentrations (MIC) and minimum bactericidal concentrations (MBC) were determined, with collective results shown in Fig. 6, and complete data provided in Tables ESI-4 and 5† (MIC) and Tables ESI-6 and 7† (MBC).

A general enhancement in antimicrobial performance was observed for all MET-containing metal complexes compared to metronidazole alone, across both Gram-positive and Gram-negative strains. This result is relevant, given that metronidazole is primarily effective against anaerobic pathogens;[67] thus, its weak activity against the aerobic and facultative aerobic strains tested here is consistent with expectations. Overall, the incorporation of metronidazole into the metal-salicylate framework significantly enhances the antimicrobial activity of the antibiotic towards these aerobic and facultative pathogens, making the metal complexes promising candidates for further development as broad-spectrum antimicrobial agents. The observed improvements are particularly notable for the [Ag(Sal)(MET)] complex, which consistently demonstrated the lowest MIC and MBC values across all tested bacterial strains, suggesting potential for applications in combating multidrug-resistant pathogens. This is especially promising in light of the urgent need for new agents effective against Gram-negative bacteria,[68] a category notoriously resistant to treatment due to the cell wall structure of the additional outer membrane.

Interesting considerations can be made when comparing the antimicrobial activity of the parent metal-salicylate

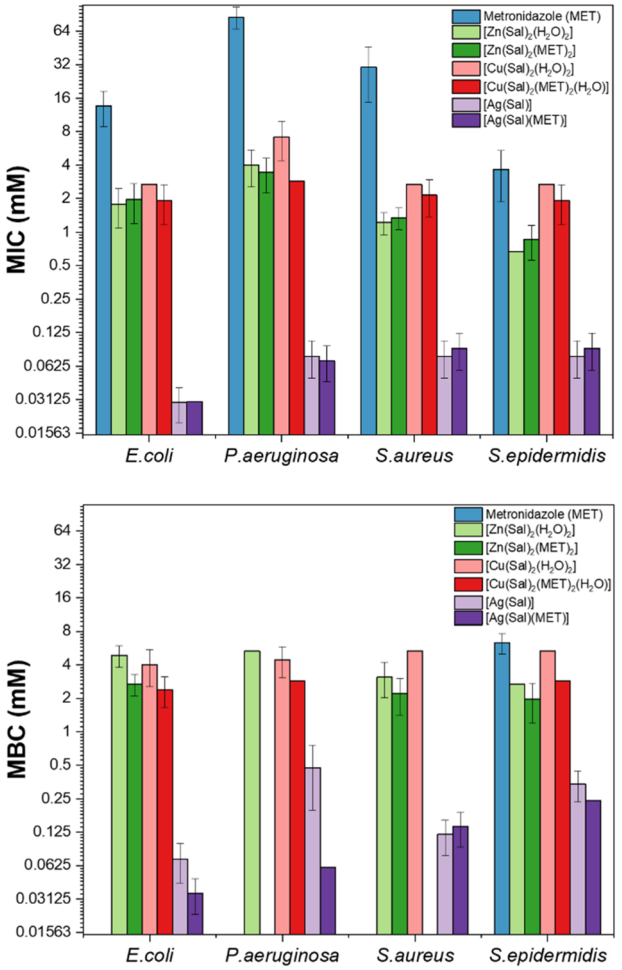

Fig. 6 (Top) Minimum inhibitory concentration (MIC), and (bottom) Minimum bactericidal concentration (MBC) for the compounds under study. The *y*-axis scale is $\log_2$ to provide better data visualization. Note: the shorter the bar, the better the antimicrobial activity.

complex with the novel metronidazole derivative prepared in this work. The $[Zn(Sal)_2(H_2O)_2]$ complex exhibited MICs in the range of 1–5 mM and MBCs between 2–3 mM. Its MET-containing analogue, $[Zn(Sal)_2(MET)_2]$, showed comparable activity with only minor variation depending on the bacterial species, indicating that metronidazole incorporation did not significantly alter the antimicrobial activity of the Zn(II)-based complex. A similar pattern was observed for the copper(II) complexes. Copper generally shows a higher antimicrobial activity with respect to zinc, however, the MIC and MBC values for both metal systems were comparable in our study. This may suggest a mitigating role of ligand environment.

Overall, the metal-salicylate framework appears to be the dominant contributor to antimicrobial action, as the inclusion of metronidazole does not drastically improve or diminish the antimicrobial activity of the parent metal-salicylate, other than for the MBC of the silver forms to the Gram-negative bacteria. This prompted further investigation into potential synergistic or antagonistic effects.

Fractional inhibitory concentration index (FIC index)

To assess possible synergistic or antagonistic effects in combining metronidazole with the metal-salicylate complex, FIC indices were calculated for combinations of MET with $[Zn(Sal)_2(H_2O)_2]$, $[Cu(Sal)_2(H_2O)_2]$ and [Ag(Sal)], against *P. aeruginosa* and *S. epidermidis*. The choice of the pathogen used in these experiments was based on which displayed the higher (*S. epidermidis*) and lower (*P. aeruginosa*) antimicrobial response toward the tested compounds.

As shown in Fig. 7, the results are considerably different for these two very physiologically different bacteria. For *P. aeruginosa*, synergy was observed for MET in combination with $[Zn(Sal)_2(H_2O)_2]$ and [Ag(Sal)], whereas the combination with the copper equivalent: $[Cu(Sal)_2(H_2O)_2]$ exhibited only additive effects. In contrast, against *S. epidermidis*, the MET-$[Zn(Sal)_2(H_2O)_2]$ combination was indifferent, while the Cu(II) and Ag(I) complexes again yielded additive effects. Overall, the FIC index analysis suggests that the combination of metronidazole with most metal-salicylates demonstrates potential synergistic or additive effects against both *P. aeruginosa* and *S. epidermidis*.

While these interactions are informative for co-administration of unbound components, they do not directly translate to the activity of the coordinated MET–metal complexes. This is likely due to the fact that in the synthesized complexes, MET is coordinated to the metal centre and thus not freely available in solution. Coordination alters both the electronic structure and reactivity of the ligand, which may suppress the individual synergistic effects observed in binary mixtures.

Biofilm inhibition

Although most compounds displayed a concentration of complete inhibition of bacteria growth (MBC assay), this does not preclude the possibility of biofilm formation during incubation, given the high antimicrobial tolerance of biofilms.[69]

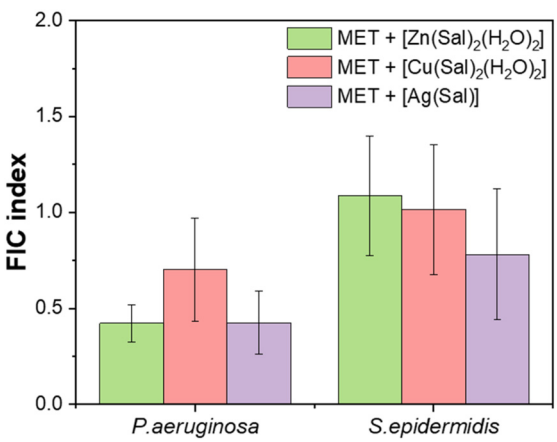

Fig. 7 Fractional inhibitory concentration (FIC) index of metronidazole (MET) in combination with metallo-salicylates ($[Zn(Sal)_2(H_2O)_2]$, $[Cu(Sal)_2(H_2O)_2]$, and [Ag(Sal)]) against representative strains of *P. aeruginosa* and *S. epidermidis*.

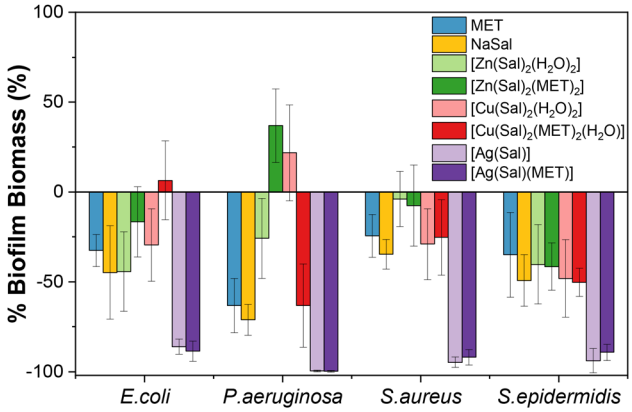

Fig. 8 Antibiofilm activity of the compounds under study at 0.1 mg mL^{-1} of compound.

To evaluate anti-biofilm properties, all compounds were tested at a uniform concentration of 0.1 mg mL^{-1}, regardless of their MIC or MBC values, to enable cross-comparison. As shown in Fig. 8, exposure to this sub-MIC concentration resulted in measurable reductions in biofilm biomass for all tested strains, even in the case of metronidazole, whose MICs were substantially higher. Intriguingly, similar results are observed also for sodium salicylate, despite no bactericidal nor bacteriostatic action was observed during the other antimicrobial tests. However, in some cases, an increase in biofilm biomass was observed. For instance, exposure of *P. aeruginosa* to [Zn(Sal)$_2$(MET)$_2$] led to enhanced biofilm formation. This phenomenon is consistent with known bacterial responses to sublethal stress, wherein *P. aeruginosa* may upregulate the production of extracellular polymeric matrix as a protective mechanism.

Conclusions

This study reports the synthesis and structural characterization of a series of metronidazole-based metal complexes incorporating salicylate ligands and Zn(II), Cu(II), or Ag(I) ions. Single-crystal X-ray diffraction revealed the existence of polymorphic forms for both the zinc and copper complexes, with the most thermodynamically stable forms (**1b** and **2b**, respectively) being readily obtained through bulk methods such as mechanochemistry and slurry.

Antimicrobial assays demonstrated that metal complex formation enhances the activity of metronidazole against aerobic Gram-positive and Gram-negative pathogens, with the silver complex [Ag(MET)(Sal)] (**3**) showing the most promising profile, including low MIC and MBC values and effective biofilm inhibition. Interestingly, for the Zn(II) and Cu(II) complexes, incorporation of metronidazole did not significantly alter the antimicrobial efficacy compared to their parent metal-salicylates.

Without extensive omics and biochemical studies, it is premature to propose a definitive mechanism of action; however, a plausible hypotheses can be postulated based on existing knowledge. Salicylic acid may facilitate MET entry into the bacterial cell by altering the transporters that are regulated by the mar regulon.[70] Additionally, salicylic acid depolarizes the bacterial membrane, leading to loss of energy needed for proton-motif force (PMF) dependent efflux pumps; as a result, intracellular MET is not effluxed. The presence of the metal centre also has an action: silver ions are known to damage redox enzymes, releasing iron that catalyses reactive oxygen species (ROS) production *via* Fenton-type reactions. This oxidative stress can damage membranes[12] Similarly, copper exhibits Fenton reactivity, while zinc interferes with thiol biochemistry: exposure to both metal ions would lead to ROS generation. Furthermore, all three metals, could work with salicylic acid to effectively damage the electron transport chain proteins, further uncoupling the PMF.

Although bacterial membranes differ in lipid composition, their characteristics are overall similar. Bacterial membranes contain more negatively charged head groups than eukaryotic membranes, with the acyl chains being similar in length and saturation profiles, and similar membrane dynamic properties are expected across strains. Thus, differences in the lipophilicity of our compounds, as described by structure–activity relationship (SAR), would not be expected to differentially affect the bacteria. Instead, species-specific differences in the efficacies of our compounds likely stem from the presence or absence of key transporters and from variations in the abundance and susceptibility of reactive thiol-containing (RSH) enzymes. Moving forward, although salicylic acid, metronidazole and the individual metals all have established toxicological profiles, the safety of each metal complex would need to be independently evaluated for any intended application.

Regardless, the findings presented here are particularly promising considering the limited antimicrobial activity of metronidazole against aerobic pathogens. Future studies will extend this investigation to anaerobic bacterial pathogens, for which metronidazole is known to be clinically active, in order to further explore the applicational potential of these novel metal complexes.

Author contributions

Laura Contini: investigation, formal analysis, methodology, writing – original draft; Fabrizia Grepioni and Ray J. Turner: conceptualization, supervision, investigation, formal analysis, methodology, writing, resources.

Conflicts of interest

The authors declare no conflicts of interest.

Data availability

The data supporting this article have been included as part of the ESI.†

Acknowledgements

The PNRR DM 351/2022 PhD project (LC) is acknowledged. FG acknowledges financial support from MUR, project "NICE – Nature Inspired Crystal Engineering" (PRIN2020) and financial support (RFO) from the University of Bologna. RJT acknowledges a Discovery Grant from the National Sciences and Engineering Research Council (NSERC) of Canada.

References

1 F. Prestinaci, P. Pezzotti and A. Pantosti, *Pathog. Global Health*, 2015, **109**, 309–318.
2 K. W. K. Tang, B. C. Millar and J. E. Moore, *Br. J. Biomed. Sci.*, 2023, **80**, 11387.
3 G. Muteeb, M. T. Rehman, M. Shahwan and M. Aatif, *Pharmaceuticals*, 2023, **16**, 1615.
4 S. Solanki and H. K. Das, *J. Med. Surg. and Public Health*, 2024, **3**, 100122.
5 C. S. Ho, C. T. H. Wong, T. T. Aung, R. Lakshminarayanan, J. S. Mehta, S. Rauz, A. McNally, B. Kintses, S. J. Peacock, C. de la Fuente-Nunez, R. E. W. Hancock and D. S. J. Ting, *Lancet Microbe*, 2025, **6**(1), 100947, DOI: **10.1016/j.lanmic.2024.07.010**.
6 P. Dadgostar, *Infect. Drug Resist.*, 2019, **12**, 3903–3910.
7 C. J. L. Murray, K. S. Ikuta, F. Sharara, L. Swetschinski, G. R. Aguilar, A. Gray, C. Han, C. Bisignano, P. Rao, E. Wool, S. C. Johnson, A. J. Browne, M. G. Chipeta, F. Fell, S. Hackett, G. Haines-Woodhouse, B. H. K. Hamadani, E. A. P. Kumaran, B. McManigal, S. Achalapong, R. Agarwal, S. Akech, S. Albertson, J. Amuasi, J. Andrews, A. Aravkin, E. Ashley, F.-X. Babin, F. Bailey, S. Baker, B. Basnyat, A. Bekker, R. Bender, J. A. Berkley, A. Bethou, J. Bielicki, S. Boonkasidecha, J. Bukosia, C. Carvalheiro, C. Castañeda-Orjuela, V. Chansamouth, S. Chaurasia, S. Chiurchiù, F. Chowdhury, R. C. Donatien, A. J. Cook, B. Cooper, T. R. Cressey, E. Criollo-Mora, M. Cunningham, S. Darboe, N. P. J. Day, M. D. Luca, K. Dokova, A. Dramowski, S. J. Dunachie, T. D. Bich, T. Eckmanns, D. Eibach, A. Emami, N. Feasey, N. Fisher-Pearson, K. Forrest, C. Garcia, D. Garrett, P. Gastmeier, A. Z. Giref, R. C. Greer, V. Gupta, S. Haller, A. Haselbeck, S. I. Hay, M. Holm, S. Hopkins, Y. Hsia, K. C. Iregbu, J. Jacobs, D. Jarovsky, F. Javanmardi, A. W. J. Jenney, M. Khorana, S. Khusuwan, N. Kissoon, E. Kobeissi, T. Kostyanev, F. Krapp, R. Krumkamp, A. Kumar, H. H. Kyu, C. Lim, K. Lim, D. Limmathurotsakul, M. J. Loftus, M. Lunn, J. Ma, A. Manoharan, F. Marks, J. May, M. Mayxay, N. Mturi, T. Munera-Huertas, P. Musicha, L. A. Musila, M. M. Mussi-Pinhata, R. N. Naidu, T. Nakamura, R. Nanavati, S. Nangia, P. Newton, C. Ngoun, A. Novotney, D. Nwakanma, C. W. Obiero, T. J. Ochoa, A. Olivas-Martinez, P. Olliaro, E. Ooko, E. Ortiz-Brizuela, P. Ounchanum, G. D. Pak, J. L. Paredes, A. Y. Peleg, C. Perrone, T. Phe, K. Phommasone, N. Plakkal, A. Ponce-de-Leon, M. Raad, T. Ramdin, S. Rattanavong, A. Riddell, T. Roberts, J. V. Robotham, A. Roca, V. D. Rosenthal, K. E. Rudd, N. Russell, H. S. Sader, W. Saengchan, J. Schnall, J. A. G. Scott, S. Seekaew, M. Sharland, M. Shivamallappa, J. Sifuentes-Osornio, A. J. Simpson, N. Steenkeste, A. J. Stewardson, T. Stoeva, N. Tasak, A. Thaiprakong, G. Thwaites, C. Tigoi, C. Turner, P. Turner, H. R. van Doorn, S. Velaphi, A. Vongpradith, M. Vongsouvath, H. Vu, T. Walsh, J. L. Walson, S. Waner, T. Wangrangsimakul, P. Wannapinij, T. Wozniak, T. E. M. W. Young Sharma, K. C. Yu, P. Zheng, B. Sartorius, A. D. Lopez, A. Stergachis, C. Moore, C. Dolecek and M. Naghavi, *Lancet*, 2022, **399**, 629–655, DOI: **10.1016/S0140-6736(21)02724-0**.
8 Antimicrobial Resistance Division (AMR), Global Coordination and Partnership (GCP), Medicines Selection, IP and Affordability (MIA), 2017.
9 S. K. Gupta and R. P. Nayak, *J. Pharmacol. Pharmacother.*, 2014, **5**, 4–7.
10 Global Observatory on Health R&D, Antibacterial products in clinical development for priority pathogens, **https://www.who.int/observatories/global-observatory-on-health-research-and-development/monitoring/antibacterial-products-in-clinical-development-for-priority-pathogens**, (accessed 21 April 2025).
11 J. E. Waters, L. Stevens-Cullinane, L. Siebenmann and J. Hess, *Curr. Opin. Microbiol.*, 2023, **75**, 102347.
12 J. A. Lemire, J. J. Harrison and R. J. Turner, *Nat. Rev. Microbiol.*, 2013, **11**, 371–384.
13 T. C. Johnstone, K. Suntharalingam and S. J. Lippard, *Chem. Rev.*, 2016, **116**, 3436–3486.
14 F. Bosch and L. Rosich, *Pharmacology*, 2008, **82**, 171–179.
15 C. Roder and M. J. Thomson, *Drugs R D*, 2015, **15**, 13–20, DOI: **10.1007/s40268-015-0083-y**.
16 D. A. Geier, L. K. Sykes and M. R. Geier, *J. Toxicol. Environ. Health, Part B*, 2007, **10**, 575–596.
17 C. Biot, F. Nosten, L. Fraisse, D. Ter-Minassian, J. Khalife and D. Dive, *Parasite*, 2011, **18**, 207–214.
18 R. G. Kenny and C. J. Marmion, *Chem. Rev.*, 2019, **119**, 1058–1137.
19 R. J. Turner, *BioMetals*, 2024, **37**, 545–559.
20 A. Frei, A. D. Verderosa, A. G. Elliott, J. Zuegg and M. A. T. Blaskovich, *Nat. Rev. Chem.*, 2023, **7**, 202–224.
21 R. J. Turner, *Microb. Biotechnol.*, 2017, **10**, 1062–1065.
22 D. A. Salazar-Alemán and R. J. Turner, in *Microbial Metabolism of Metals and Metalloids*, ed. C. J. Hurst, Springer International Publishing, Cham, 2022, pp. 77–106.
23 A. Frei, J. Zuegg, A. G. Elliott, M. Baker, S. Braese, C. Brown, F. Chen, C. G. Dowson, G. Dujardin, N. Jung, A. P. King, A. M. Mansour, M. Massi, J. Moat, H. A. Mohamed, A. K. Renfrew, P. J. Rutledge, P. J. Sadler, M. H. Todd, C. E. Willans, J. J. Wilson, M. A. Cooper and M. A. T. Blaskovich, *Chem. Sci.*, 2020, **11**, 2627–2639.
24 S. Domingos, V. André, S. Quaresma, I. C. B. Martins, M. F. Minas da Piedade and M. T. Duarte, *J. Pharm. Pharmacol.*, 2015, **67**, 830–846.

25 G. Gasser, *Chimia*, 2015, **69**, 442–442.
26 G. Gasser and N. Metzler-Nolte, *Curr. Opin. Chem. Biol.*, 2012, **16**, 84–91.
27 T. Gianferrara, I. Bratsos and E. Alessio, *Dalton Trans.*, 2009, 7588–7598.
28 S. A. Dingsdag and N. Hunter, *J. Antimicrob. Chemother.*, 2018, **73**, 265–279.
29 A. Smith, *Br. Dent. J.*, 2018, **224**, 403–404.
30 L. Boyanova, P. Hadzhiyski, R. Gergova and R. Markovska, *Antibiotics*, 2023, **12**, 332.
31 M. Bashimam and H. El-Zein, *Heliyon*, 2022, **8**, e11872.
32 W. A. A. Saleh and N. M. Abbass, *Chem. Methodol.*, 2023, **7**, 81–91.
33 S.-F. Cui, L.-P. Peng, H.-Z. Zhang, S. Rasheed, V. K. Kannekanti and C.-H. Zhou, *Eur. J. Med. Chem.*, 2014, **86**, 318–334.
34 R. Seera and T. N. Guru Row, *Cryst. Growth Des.*, 2020, **20**, 4667–4677.
35 U. Kalinowska-Lis, A. Felczak, L. Chęcińska, K. Zawadzka, E. Patyna, K. Lisowska and J. Ochocki, *Dalton Trans.*, 2015, **44**, 8178–8189.
36 A. J. Dyba, E. Wiącek, M. Nowak, J. Janczak, K. P. Nartowski and D. E. Braun, *Cryst. Growth Des.*, 2023, **23**, 8241–8260.
37 C. Fiore, F. Antoniciello, D. Roncarati, V. Scarlato, F. Grepioni and D. Braga, *Pharmaceutics*, 2024, **16**, 203.
38 L. Contini, A. Paul, L. Mazzei, S. Ciurli, D. Roncarati, D. Braga and F. Grepioni, *Dalton Trans.*, 2024, **53**, 10553–10562.
39 C. Fiore, A. Lekhan, S. Bordignon, M. R. Chierotti, R. Gobetto, F. Grepioni, R. J. Turner and D. Braga, *Int. J. Mol. Sci.*, 2023, **24**, 5180.
40 S. d'Agostino, L. Macchietti, R. J. Turner and F. Grepioni, *Front. Chem.*, 2024, **12**, 1430457.
41 R. Sun, L. Casali, R. J. Turner, D. Braga and F. Grepioni, *Molecules*, 2023, **28**, 1244.
42 C. Fiore, O. Shemchuk, F. Grepioni, R. J. Turner and D. Braga, *CrystEngComm*, 2021, **23**, 4494–4499.
43 M. Guerrini, S. d'Agostino, F. Grepioni, D. Braga, A. Lekhan and R. J. Turner, *Sci. Rep.*, 2022, **12**, 3673.
44 F. Grepioni, L. Casali, C. Fiore, L. Mazzei, R. Sun, O. Shemchuk and D. Braga, *Dalton Trans.*, 2022, **51**, 7390–7400.
45 M. Kumar, A. K. Singh, V. K. Singh, R. K. Yadav, A. P. Singh and S. Singh, *Coord. Chem. Rev.*, 2024, **505**, 215663.
46 J. Cardoso, E. Pinto, E. Sousa and D. I. S. P. Resende, *J. Med. Chem.*, 2025, **68**, 5006–5023.
47 Y. Lin, H. Betts, S. Keller, K. Cariou and G. Gasser, *Chem. Soc. Rev.*, 2021, **50**, 10346–10402.
48 I. Salah, I. P. Parkin and E. Allan, *RSC Adv.*, 2021, **11**, 18179–18186.
49 N. Vishwanath, C. Whitaker, S. Allu, D. Clippert, E. Jouffroy, J. Hong, B. Stone, W. Connolly, C. C. Barrett, V. Antoci, C. T. Born and D. R. Garcia, *Surg. Infect.*, 2022, **23**, 769–780.
50 J. C. Ballin, *J. Am. Med. Assoc.*, 1974, **230**, 1184–1185.
51 K. Kalantari, E. Mostafavi, A. M. Afifi, Z. Izadiyan, H. Jahangirian, R. Rafiee-Moghaddam and T. J. Webster, *Nanoscale*, 2020, **12**, 2268–2291.
52 A.-C. Burduşel, O. Gherasim, A. M. Grumezescu, L. Mogoantă, A. Ficai and E. Andronescu, *Nanomaterials*, 2018, **8**, 681.
53 M. Muller and N. D. Merrett, *Antimicrob. Agents Chemother.*, 2014, **58**, 5492–5499.
54 A. Panáček, L. Kvítek, M. Smékalová, R. Večeřová, M. Kolář, M. Röderová, F. Dyčka, M. Šebela, R. Prucek, O. Tomanec and R. Zbořil, *Nat. Nanotechnol.*, 2018, **13**, 65–71.
55 A. E.-D. M. Hosny, S. A. Rasmy, D. S. Aboul-Magd, M. T. Kashef and Z. E. El-Bazza, *Infect. Drug Resist.*, 2019, **12**, 1985–2001.
56 A. B. Turner, E. Gerner, R. Firdaus, M. Echeverz, M. Werthén, P. Thomsen, S. Almqvist and M. Trobos, *Front. Microbiol.*, 2022, **13**, 931839.
57 T. Friščić, C. Mottillo and H. M. Titi, *Angew. Chem., Int. Ed.*, 2020, **59**, 1018–1029.
58 G. M. Sheldrick, *Acta Crystallogr., Sect. A:Found. Adv.*, 2015, **71**, 3–8.
59 G. M. Sheldrick, *Acta Crystallogr., Sect. C:Struct. Chem.*, 2015, **71**, 3–8.
60 O. V. Dolomanov, L. J. Bourhis, R. J. Gildea, J. a. K. Howard and H. Puschmann, *J. Appl. Crystallogr.*, 2009, **42**, 339–341.
61 C. F. Macrae, I. Sovago, S. J. Cottrell, P. T. A. Galek, P. McCabe, E. Pidcock, M. Platings, G. P. Shields, J. S. Stevens, M. Towler and P. A. Wood, *J. Appl. Crystallogr.*, 2020, **53**, 226–235.
62 S. L. Tan, M. M. Jotani and E. R. T. Tiekink, *Acta Crystallogr., Sect. E:Crystallogr. Commun.*, 2019, **75**, 308–318.
63 C. F. Mackenzie, P. R. Spackman, D. Jayatilaka and M. A. Spackman, *IUCrJ*, 2017, **4**, 575–587.
64 P. R. Spackman, M. J. Turner, J. J. McKinnon, S. K. Wolff, D. J. Grimwood, D. Jayatilaka and M. A. Spackman, *J. Appl. Crystallogr.*, 2021, **54**, 1006–1011.
65 F. C. Odds, *J. Antimicrob. Chemother.*, 2003, **52**, 1.
66 European Committee for Antimicrobial Susceptibility Testing (EUCAST) of the European Society of Clinical Microbiology and Infectious Diseases (ESCMID), *Clin. Microbiol. Infect.*, 2000, **6**, 503–508.
67 S. Löfmark, C. Edlund and C. E. Nord, *Clin. Infect. Dis*, 2010, **50**, S16–S23.
68 Z. Breijyeh, B. Jubeh and R. Karaman, *Molecules*, 2020, **25**, 1340.
69 J. J. Harrison, H. Ceri and R. J. Turner, *Nat. Rev. Microbiol.*, 2007, **5**, 928–938.
70 E. M. E. Sykes, D. White, S. McLaughlin and A. Kumar, *Can. J. Microbiol.*, 2024, **70**, 1–14.